Introduction of localized spin-state transitions in the optical absorption spectrum of Cr-doped GaN

Masoud Mansouri [1,2,3,*] D. Kirk Lewis,[3,†] and Sahar Sharifzadeh [3,4,‡]

[1]*Donostia International Physics Center (DIPC), Paseo Manuel de Lardizabal, 4, 20018 Donostia-San Sebastián, Spain*
[2]*Centro de Física de Materiales, Centro Mixto CSIC-UPV/EHU, Paseo Manuel de Lardizabal, 5, 20018 Donostia-San Sebastián, Spain*
[3]*Department of Electrical and Computer Engineering, Boston University, Boston, Massachusetts 02215, USA*
[4]*Division of Materials Science and Engineering, Boston University, Boston, Massachusetts 02215, USA*

Using a hybrid density functional, we study the electronic, magnetic, and neutral excitations of the paradigmatic Cr-doped GaN solid. Our results indicate that the $\approx 1\%$ doped wurtzite GaN crystal retains the semiconducting nature of the host, associated with a magnetic moment of 3 μ_B. As a consequence of Cr doping, additional hybridized bands are formed within the intrinsic band gap of GaN, leading to a considerable band gap narrowing by 1.4 eV and low-energy optical transitions. Our results indicate dark Cr d-d transitions at very low energy (0.5–0.7 eV), followed by bright transitions in the visible energy range (1.8–2.2 eV). Characterization of the electron-hole pairs suggests that the latter originates from the internal transitions among hybridized Cr_d–N_p states. With the existence of these additional optical features within the visible energy window, one can expect an enhancement to the photoelectric conversion efficiency of GaN upon Cr doping, in addition to applications in spintronics.

I. INTRODUCTION

Transition metal doping of gallium nitride (GaN) has been shown to alter its intrinsic electronic structural and optical features by the introduction of deep donor and/or acceptor levels [1–11]. Additionally, the presence of open-shell transition metals can result in magnetic properties [11–14]. For instance, adding chromium (Cr) dopant(s) into the host GaN matrix leads to the alignment of magnetic domains in the same direction, which causes spin polarization and ferromagnetism with a relatively high Curie temperature [1–4,11]. Such an additional functionality suggests Cr-doped GaN is a robust and promising material in the field of diluted magnetic semiconductors, particularly for spintronic and quantum information applications which typically require localized spin states [10,11,15,16].

Cr impurities within the GaN crystal introduce low-energy excited states, stemming from dopant-induced charge carrier traps and recombination centers within the intrinsic gap [1,8]. As a result, an extra optical absorption spectrum has been observed over the *visible* energy window, attributed to the internal transitions among Cr-d states [1,7,9,17]. The existence of these states in the gap is due to the Jahn-Teller effect [8], where spatially degenerate Cr-d states distort and split in energy due to the interaction with the crystal field of the host environment, forming midgap energy bands which act as trapping centers for both holes and electrons [1,7] and lead to low-energy transitions in the optical spectrum. Moreover,

the presence of hybridized near-gap states of Cr-d/N-p character can result in a decrease of energy loss through heat [7], potentially enhancing the photoelectric conversion efficiency.

Despite its technological relevance, the underlying electronic structure involved in the optically excited states of Cr-doped GaN is not well understood. While electrical resistivity measurements suggest the Cr-doped GaN in the low-doping regime is semiconducting [13,18], most theoretical studies based on first-principles density functional theory (DFT) predict half-metallic phases [6,14,19], even with the addition of on-site correlation effects via a Hubbard correction [3,12]. Additionally, due to the presence of self-interaction error in DFT with (semi)local exchange-correlation functionals [20], localized electronic states such as those associated with Cr d states may be overly delocalized, unphysically increasing the defect-defect interactions. To describe optical properties and excitonic effects in the solid states, moreover, a more complex nonlocal functional is needed [21]. Thus, it is necessary to go beyond local and semilocal DFT to understand the electronic and optical properties of Cr-doped GaN [22].

Recently, some of us have established the accuracy of different computational techniques in the prediction of the fundamental gap and optically excited states of the pristine and defective GaN solids [23] and showed that a tuned and screened range-separated hybrid functional (SRSH) [24,25] applied within DFT and its time-dependent extension (TDDFT) successfully reproduces the band structure and optical absorption spectrum of pristine and defective GaN predicted from many-body perturbation theory within the GW/BSE approximation [21,26], and the experimental absorption spectrum of pristine GaN [23]. Here, we analogously apply the SRSH functional within the DFT/TDDFT framework to study $\approx 1\%$ substitutional Cr:GaN, with the goal of

*ma.mansouri@dipc.org
†kirk@bu.edu
‡ssharifz@bu.edu

understanding the dopant-induced trap states and low-energy excitonic peaks. Our calculated results show that the electronic structure of the bulk Cr-doped GaN in the low-doping regime remains in the semiconducting phase while band edges are largely formed by dopant d states. In particular, we find that the valence edge consists of the three unpaired bands, with energies spanning 1.4 eV, resulting in a considerably smaller band gap with respect to the pristine GaN crystal. As a consequence of band gap narrowing, the optical absorption spectrum features a set of extra excitations which are involved in the dopant d-state transitions. Excluding the weakly allowed d-d transitions within the infrared region, we determine the low-energy peaks in the optical absorption spectrum are mixed transitions involving Cr-d states with bulk-like states, resulting in optically excited states in the visible energy window.

II. COMPUTATIONAL DETAILS

Collinear spin-polarized DFT and TDDFT calculations were performed within the VASP package [27]. We used a plane-wave cutoff of 400 eV, a Γ-centered sampling of $4\times4\times4$ in the Brillouin zone, which converged the total energy to less than 1 meV, and the projector augmented wave potentials for describing the core and nuclei [28]. A tuned functional based on that of Heyd, Scuseria, and Ernzerhof (HSE) [29] functional and the SRSH functional, as implemented by Ramasubramaniam and coworkers [23–25], were utilized to describe the exchange-correlation functional. Following prior work [30], the fraction of exact exchange in the SRSH (HSE) is set to 25% (30%) reproducing the experimental band gap of 3.5 eV [5,31]. Moreover, the range separation parameter within HSE is kept at 0.2 Å^{-1}, while for the SRSH functional, the range separation parameter, beyond which the functional is the screened exact exchange, is tuned to 0.7 Å^{-1}. The dielectric constant of GaN, used as a parameter in SRSH, is obtained from the random phase approximation [23] to be 5.4 ϵ_0 where ϵ_0 denotes the vacuum permittivity.

The structure of the pristine wurtzite GaN was adopted from recent studies [23,32]. Recent x-ray diffraction studies have confirmed a similar wurtzite structure for Cr-doped GaN crystal [7] with lattice vectors slightly larger than that of pristine GaN [33], presumably due to the larger atomic radius of Cr than Ga. It has been determined that Cr forms a substitutional defect, replacing Ga in the crystal [2,4,19,34]. Thus, we constructed a $4\times4\times3$ bulk supercell (Ga$_{96}$N$_{96}$) and substituted one of the Ga host atoms for a Cr ([Ar] $3d^5$ $4s^1$), corresponding to a $1/96 \simeq 1\%$ atomic doping ratio and concentration of 4.5×10^{20} cm^{-3}. Previously, we have shown that a $4\times4\times3$ supercell is sufficient for minimizing the interactions between periodic defects in GaN [30]. Additionally, the simulated supercell provides a separation of at least 1 nm between periodically repeating Cr dopants, much larger than the required critical separation of 2.7 Å for Cr-Cr ferromagnetic coupling [2]. The geometry of all the defective structures (neutral and charged Cr-doped GaN) was optimized using the tuned HSE 30% functional and a Γ-centered k-mesh sampling of $2\times2\times2$, converging the total energy and interatomic forces to less than 10^{-5} eV and 0.01 eV/Å, respectively. The lattice

vectors of the wurtzite relaxed (neutral) Cr-doped GaN supercell were determined to be $a = 12.8$ and $c = 15.6$ Å.

The electronic band structure was computed along a k path as defined by Ref. [35], for which the initial eigenenergies were interpolated by localized Wannier functions [36]. The charge population was computed by means of Bader analysis as implemented in Ref. [37], using both core and valence electron densities. Bader charge analysis, which evaluates the electron density remainder around the nucleus as well as the actual charge density [38–40], has previously been used to provide a good qualitative understanding of the charge state in transition-metal-doped oxides [41–43]. Optical spectra and neutral excitation energies of the doped crystal were calculated by a time-dependent kernel of both SRSH (TD-SRSH) and HSE 30% (TD-HSE) functionals. In doing so, we solved the Casida equation [21], taking into account 24 valence and 24 conduction bands.

We note that SRSH has been shown to be accurate in predicting the band structure and optical absorption properties of molecular and inorganic solids [44–48]. To gain a better understanding of the SRSH accuracy in describing d electrons, when tuned to the sp band, we have computed the Ga d-sp band splitting with $3d$ electrons explicitly included as valence in the Ga pseudopotential. The SRSH-predicted Ga-$3d$ band is found in the energy range of 13–17.5 eV below the sp-type valence band maximum (VBM), reaching its peak at ≈17 eV. This is in good agreement with the experimental peak value of 17–18 eV [49,50], measured for a wurtzite GaN thin film at room temperature (see Fig. S13). More details, including a comparison to the experimental spectrum, can be found in the Supplemental Material [51].

III. RESULTS

A. Cr-induced in-gap states in GaN

The structure of GaN is perturbed with the introduction of the Cr dopant (see Ref. [51] for the ball-and-stick model of the relaxed Cr:GaN supercell with a doping ratio of $\approx1\%$). The lattice vectors of doped GaN are slightly increased by doping (0.01%), in agreement with prior studies [33]. The presence of Cr pushes neighboring N atoms away, closer to their neighboring Ga atoms. As a result, Cr-N bond lengths are increased by approximately 2% with respect to the average bond length of host Ga-N, determined to be ≈1.95 Å. The bond angles are also modified. While N-Ga-N bond angles are approximately 109°, the N-Cr-N angle is increased to $\approx114°$. Similar to previous findings for Mn in GaN [22], although the perturbation due to the defect is not significant, there is a distortion of the nearest neighbor and next-nearest neighbor bonds to the defect, which results in electronic states as discussed below.

The total magnetic moment of the system is predicted to be 3.00 μ_B with most of the magnetic moment (2.83 μ_B) on the Cr dopant, in agreement with other first-principles-based studies [2,3,7,11,19]. This sizable magnetic moment on Cr induces a small antiferromagnetic polarization of -0.04 μ_B among the near-neighbor N atoms. Surrounding Ga atoms also feature a small magnetization of 0.01 μ_B. This behavior was attributed to the effect of through-bond spin polarization [3,6]. Using
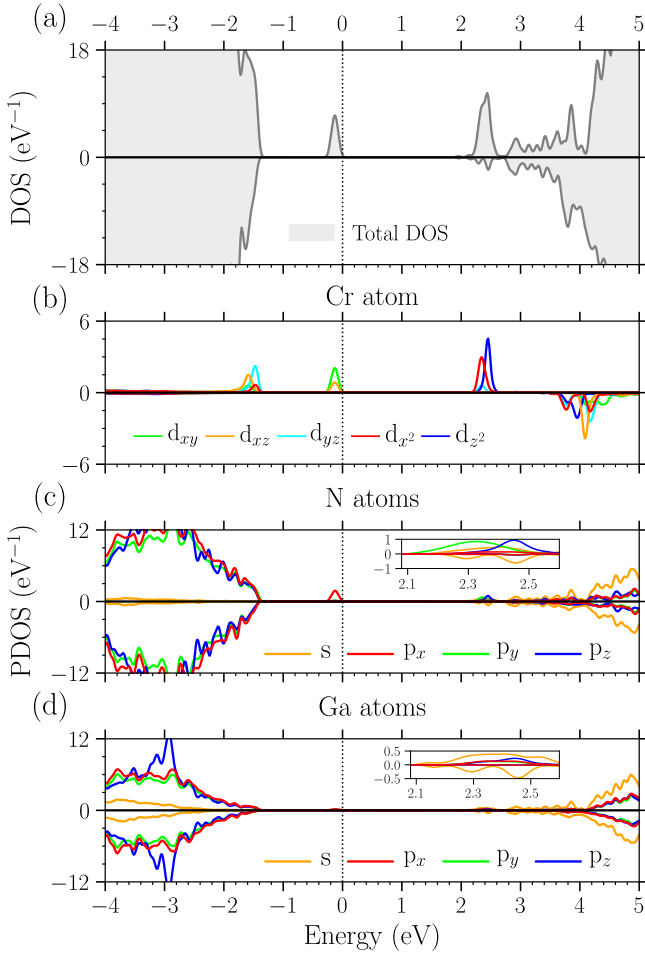
FIG. 1. Spin-resolved (a) DOS and projected DOS onto (b) Cr-d, (c) N, and (d) Ga atomic orbitals. Positive and negative values represent the majority ($\uparrow$) and minority ($\downarrow$) states. The highest occupied state energy is set to zero.

Bader analysis, moreover, we found that Cr takes a nearly trivalent form with a charge deficiency of $\approx 2.2\ |e|$ on Cr, similar to that of the host Ga atoms, while nitrogen atoms feature an anionic character. The Cr^{+3} configuration can be explained by the fact that Cr substitutes for Ga and is also compatible with previous reports both theoretically [3,6,12,41] and experimentally [7,13]. However, we should note that a few prior studies have reported a Cr^{+4} configuration in Cr-doped GaN [8,9]; to address this and gain insight into the thermodynamic transition levels, we also studied different charged states of the dopant in Sec. III C.

We predict that GaN retains its *semiconducting* nature upon Cr doping. The dopant introduces unpaired spins within the intrinsic gap of GaN as shown by the SRSH spin-polarized density of states (DOS) in Fig. 1(a), reducing the effective gap from 3.5 to ≈ 2 eV. The highest occupied state is associated with a singly occupied peak, at least 1.4 eV higher in energy than a large DOS closed-shell peak reminiscent of the pristine GaN valence band (VB). The presence of this peak is in agreement with recent photoemission spectroscopy measurements, which indicate a shift of 1.3 eV in the ionization energy of GaN upon Cr doping (from 6.7 to 5.4 eV) [7,52].

To further understand the character of the band edges, we present the spin-resolved projected-DOS (PDOS) on Cr-d and host p and s atomic orbitals in Figs. 1(b)–1(d). Overall, the PDOS indicates that the ferromagnetic character of Cr-doped GaN is due to unpaired spins on the Cr-d states hybridized with the host nitrogen p states. The highest occupied state (in-gap state) is mainly composed of Cr-d_{xy} and N-p_x states, whereas p states of the host Ga atoms do not contribute actively to this region. Within the up-spin manifold and near the pristine GaN VB (-1.4 eV), d_{yz} and d_{xz} states of Cr play a role associated with substantial contributions of N-p and a modest admixture of Ga-p states. The fact that d_{xy}, d_{xz}, and d_{yz} orbitals strongly hybridize with N-$2p$ orbitals in Cr-doped GaN has been noted previously [3,6]. In the unoccupied manifold of states, two Cr states with d_{x^2} and d_{z^2} characters appear near the pristine-like GaN conducting edge, where host atoms show broad contributions of s atomic orbitals with a slight admixture of N-p_y and p_z at the conducting band edge.

As a salient feature within Cr-d PDOS in Fig. 1(b), integration of peaks in the majority spin channel up to the Fermi energy points toward the d^3 configuration of the Cr atom. Moreover, the distribution of the Cr states within the up-spin manifold indicates degeneracy of the Cr-d states is broken; based on the tetrahedral symmetry of the crystal field, we expect that states will be split into doubly near-degenerate e_g and triply near-degenerate t_{2g} subshells, with the e_g states positioned lower in energy than t_{2g} [2]. The Cr-d states consist of two occupied low-lying majority d_{xz} and d_{yz} orbitals degenerate in energy with the GaN bulk-like VB (-1.4 eV), one occupied majority d_{xy} orbital as the highest occupied state, and the two nearly degenerate (d_{z^2}, d_{x^2}) near the conduction band (2.3–2.4 eV). Thus, computed PDOS suggests that the t_{2g} states are lower in energy than the e_g states. This discrepancy may be explained by the fact that the quantization axis of d orbitals is not aligned with the crystal axes in the calculation. Additionally, bond distortions (tetragonal elongation) in the crystal field have been shown to modify the ordering of d states in transition metal compounds [53].

We note that similar conclusions to the above can be reached by DFT calculations within HSE-30% (see the Supplemental Material [51]). Conversely, semilocal DFT within PBEsol predicts a half-metallic ground-state character for the studied system for which the bands cross the Fermi energy for the majority spin (see Supplemental Material [51]). This finding agrees with previous (semi)local DFT studies [3,6,19,54] and underlies the importance of a nonlocal exchange-correlation functional [22]. The discrepancy between functionals is due to the self-interaction error within (semi)local DFT, which is mitigated with hybrid functionals, particularly those containing the spatially nonlocal exchange term (plus an effective screened Coulomb interaction) [22,55–57].

There are three singly occupied in-gap bands within the band structure of Cr-doped GaN [Fig. 2(a)] with relatively weak dispersion <0.3 eV, indicating a localized electron density. The topmost state is located deep within the intrinsic gap of GaN and the two others form impurity states slightly above the GaN bulk-like VB. In the unoccupied region, there are two low-dispersion bands that intersect the pristine-like conduction band minimum at 2.3–2.4 eV above the highest occupied
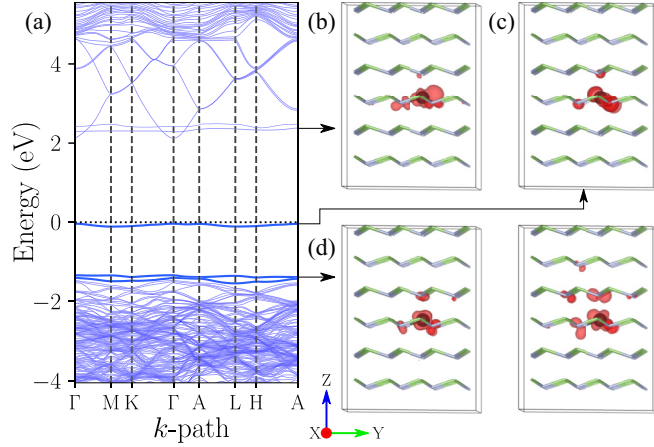
FIG. 2. (a) Spin majority electronic band structure of Cr-doped GaN crystal. Three singly occupied bands are shown in bold navy blue. The highest occupied state energy is set to zero. The charge density distributions decomposed for (b) the two lowest energy unoccupied bands, (c) the highest occupied band, and (d) the next two lower occupied bands are shown. To visualize, densities are summed over all k points and an isosurface cutoff of 10^{-3}–10^{-4} (Bohr^{-3}) was applied.
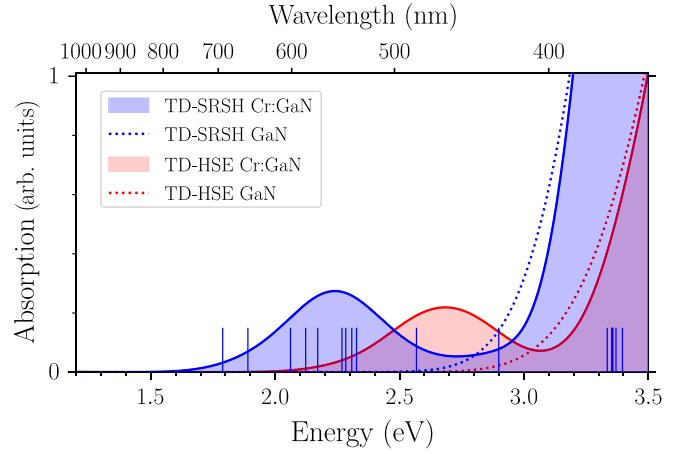

FIG. 3. Optical spectra of pristine (dotted line) and Cr-doped (shaded area) GaN solid, computed by (blue) TD-SRSH and (red) TD-HSE30%. Computed spectra are broadened with a Gaussian factor of 0.15 eV to mimic experimental resolution and the intensity was normalized such that the highest intensity in the given energy window equals one. Blue vertical bars represent the energy position of the optical transitions with remarkable oscillator strength computed by TD-SRSH for the doped crystal.

state energy. As a consequence of these in-gap states, DFT-SRSH predicts a direct band gap of 2.11 eV at Γ point that is considerably narrowed with respect to 3.5 eV for the pristine GaN [5,31]. Thus, we expect low-energy transitions in the visible energy window rather than the ultraviolet region of pristine GaN.

The reduction in the gap is due to the highest occupied band, which is localized near the Cr atom and nearest-neighbor nitrogen atoms as shown in Fig. 2(c). This is consistent with the PDOS results, Fig. 1, where we found that valence edge is made by a major contribution of Cr-d states associated with N-2p. The other two singly occupied states near the GaN VB show a similar orbital distribution through the density. For these states, however, the charge density is more evenly distributed among Cr and nearest neighbor N atoms [see Fig. 2(d)], suggesting greater hybridization of these states with the host nitrogen neighbors. The lowest unoccupied bands are a mixture of bulk-like and Cr-localized bands. We note that DFT-HSE provides qualitatively identical results, with a slightly larger band gap of 2.3 eV.

B. Low-energy optical transitions

Figure 3 presents the optical absorption spectrum of pristine and Cr-doped GaN crystals. The spectra agree well at high energies, above 3.1 eV (less than 400 nm) with a peak around 3.3–3.4 eV. The latter value is the optical absorption of the host solid, in agreement with the experimental value of 3.44 [32,58]. Within the visible energy window, both TD-SRSH and TD-HSE30% predict an additional optical structure for Cr-doped GaN, which qualitatively agrees with experimental studies that find the absorption peak associated with the defect to be 1.1–2.0 eV for a defect concentration ranging from very low to 9% doping [1,9,17]. The first bright excitation is at 1.78 eV within TD-SRSH, in excellent agreement with the ex-

perimental absorption onset of 1.62 eV [17] and 1.5 eV [1,9] for low concentration and low temperature ($T = 1.8$ K) and unintentional doping at ambient temperatures, respectively.

Given the transport gap of 2.11 eV, the exciton binding energy is determined to be 0.33 eV, reflecting the localization of the GaN Wannier-Mott-like exciton, with a binding energy of less than 100 meV [23,59]. In the energy range between 2.1 and 2.4 eV, there are a set of transitions with a peak at 2.17 eV (see blue bars representing TD-SRSH eigenvalues), reconciling the experimental value of 2.1 eV [1]. A further allowed transition with a high-exciton intensity is also found at 2.9 eV which exactly matches with experiment [1,17]. We note that there are two low-energy dark excitations (at 0.57 and 0.68 eV within TD-SRSH) with small oscillator strength. As shown in the Supplemental Material [51], these states are composed of d-d transitions, which should be symmetry forbidden but are weakly allowed due to the hybridization of Cr-d and N-2p states. To our knowledge, there is no experimental evidence of these transitions, possibly because of the low transition probability.

In a previous study on pristine and defective GaN crystals [23], some of us have shown that TD-HSE results in a blue-shifted spectrum with respect to TD-SRSH, BSE, and experiment. For Cr-doped GaN, we similarly find that the TD-HSE predicts an onset of absorption at 2.1 eV and a peak maximum at 2.7 eV. This may be ascribed to the lack of nonlocality in the long-range electron-hole correlation within the TD-HSE kernel [23].

To gain insight into the origin of the bright transitions, we inspect the coupling coefficients of electron-hole pairs along three high-symmetry k points for the three lowest bright states. For the first bright transition at 1.78 eV shown in Fig. 4(a), the largest coupling coefficients are predicted to be from the GaN bulk-like valence bands to the two lowest localized unoccupied bands with Cr-d character, and some contribution
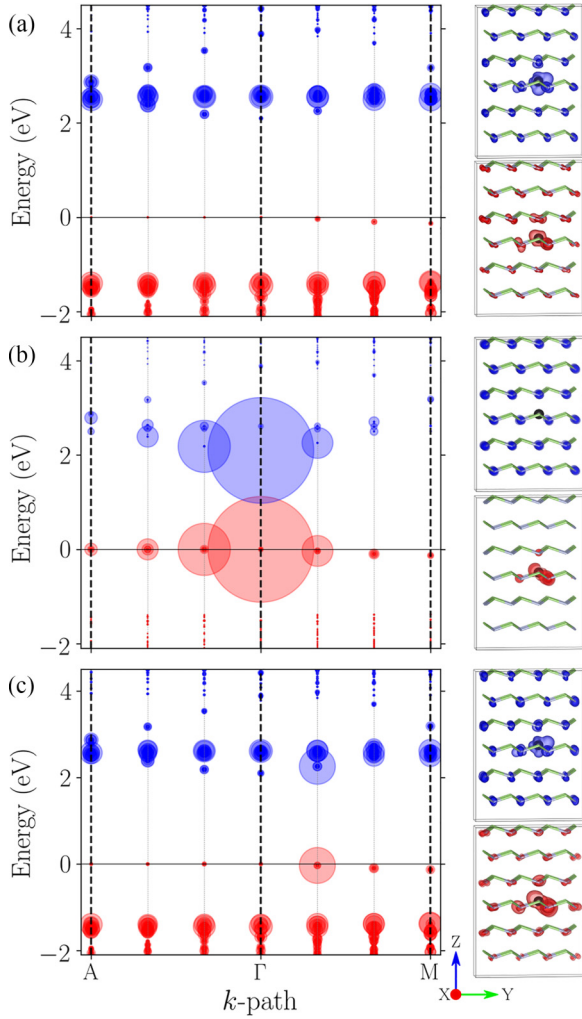
FIG. 4. Visualization of the hole (red circles) and electron (blue circles) eigenvalues contributing to the bright optically excited states at (a) 1.78, (b) 1.88, and (c) 2.17 eV. The radii of circles, representing the absolute value of the coupling coefficients, were enhanced by a factor of 35 for visualization. For each transition, the spatial distribution of the hole (red) and electron (blue) densities is shown on the right-hand side.

of transitions from shallow impurity bands to the bottom of the GaN bulk-like band. The effective orbitals associated with the electron and hole shown on the right side of the figure clearly show this mixed Cr-d/bulk-like transition; here, the electron and hole densities are distributed throughout the bulk with localization around the defect. For the next bright transition at 1.88 eV [Fig. 4(b)], the substantial contribution of the electron-hole pairs stems from d orbital to bulk-like transitions at the Γ point and results in a highly localized hole on the Cr defect and delocalized electron density. The strongest oscillation over the visible energy range is obtained for excitation energy at 2.17 eV, shown in Fig. 4(c). Similar to the 1.78-eV excitation, this state is a transition between bulk-like to defect-like states. The strong oscillator strength of these bright transitions may be explained due to the hybridization with the bulk. We also note that our predicted absorption spectrum agrees with recent experimental studies

where a low-energy peak at this energy is referred to as the fingerprint of the doping-induced effects [1,8,9,17].

C. Electronic structure of charged Cr dopants

To gain an understanding of the charged states of the Cr dopant, we simulated the electronic structure of the positively and negatively charged Cr-doped GaN, i.e., [Cr: GaN]$^{+1}$/[Cr: GaN]$^{-1}$ for which we may expect that Cr will form a +4/+2 configuration. For [Cr: GaN]$^{+1}$, DOS in Fig. 5(a) reveals two singly occupied states at the majority-spin valence edge of GaN while the deep impurity level of the neutral configuration has moved up in energy into the conducting region. As a result, the band gap of the positively charged system (3.4 eV) is determined to be close to that of pristine GaN while the magnetic moment is diminished to 2 μ_B. The PDOS and charge density distribution decomposed for band-edge states, gathered in the Supplemental Material [51], feature similar structures to the corresponding states in neutral Cr-doped GaN, although the bottom of the conduction band is more primarily composed of Cr 3d states hybridized with p states of host N atoms. As a result of the localized nature of the transition, the optical absorption of the positively charged system in the lower panel of Fig. 5(a) shows strong excitonic bonding energy with an onset of 2.3 eV stemming from transitions among GaN valence-bulk-like bands to the lowest dopant-induced unoccupied states (see Fig. S8).

For negatively charged Cr-doped GaN [Cr: GaN]$^{-1}$, the SRSH-DOS in Fig. 5(b) exhibits four half-filled states at the valence edge, originating from Cr atomic orbitals (d^4 configurations) with a magnetic moment of 4 μ_B. Compared with the neutral Cr-doped GaN, the band gap is significantly reduced to 1.2 eV due to the presence of impurity levels in the valence manifold, whereas the bottom of the conducting region is only composed of the GaN states. The only empty Cr state (d_{z^2}) falls at 2.5 eV above the VBM (see PDOS and charge distribution in the Supplemental Material [51]). As a result of the band gap narrowing, the onset of the optical absorption spectrum for [Cr: GaN]$^{-1}$ occurs at 1.02 eV followed by a peak at 1.36 eV and a broadened spectrum over the whole visible window. Inspecting the coupling coefficients of electron-hole pairs in Fig. S12 for these bright states confirms that the most significant coupling coefficients stem from the transition between the two topmost Cr-impurity levels in the valence region and the GaN bulk-like conduction bands.

At higher energies (>3 eV), we have found a roughly comparable character in the optical structure of both charged systems to the neutral Cr: GaN or the pristine GaN systems. Over this region, TD-SRSH predicts a set of transitions whose highest coefficients are determined to be at about 3.3 eV, which can be tentatively attributed to the intrinsic excitations of the pure GaN.

For completeness, we have also calculated the thermodynamic transition levels for both charged defects as $\varepsilon(q_1/q_2) = E_{q_1}^{tot} - E_{q_2}^{tot} - E_V$, where E_q^{tot} is the total energy of the defect in charge state q, and E_V is the valence energy of the pristine GaN. To eliminate the spurious electrostatic interaction among periodically repeating charged defects from E_q^{tot}, we applied the scheme proposed by Freysoldt *et al.* [60,61] that accounts for the electrostatic screening of the defect (see
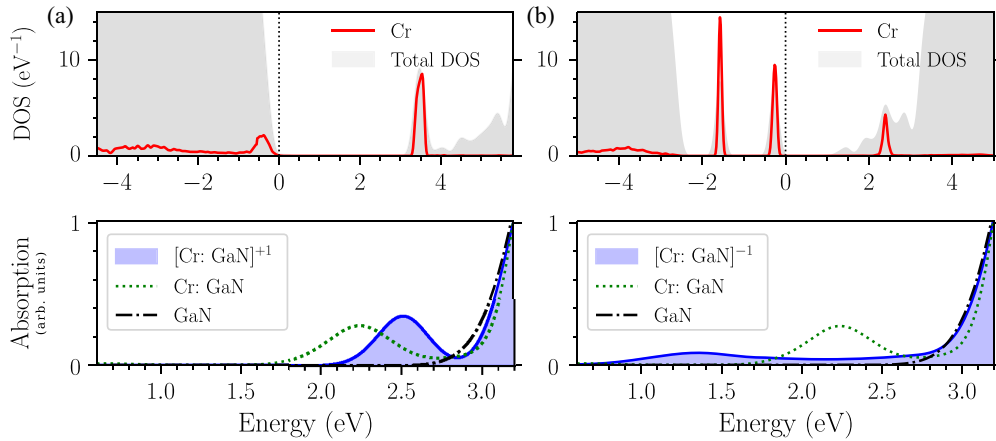
FIG. 5. Spin majority DOS and the optical absorption spectra of (a) positively and (b) negatively charged Cr-doped GaN solid. Optical spectra are broadened with a Gaussian factor of 0.15 eV and the intensity was normalized to one. For comparison, the optical spectra of pristine and neutral Cr-doped GaN in Fig. 3 are given by dashed black and dotted green lines, receptively.

Supplemental Material [51] for more details). The predicted thermodynamic transition levels of positively and negatively charged defect systems are found to be 0.94 and 2.26 eV, respectively, indicating that both charged states are within the intrinsic gap of GaN.

IV. CONCLUSION

We have investigated the electronic, magnetic, and optical properties of Cr-doped GaN using hybrid DFT and TDDFT. The solid-state range-separated hybrid functional (SRSH) predicts that a 1% Cr doping results in a semiconducting ground state with a significant magnetic moment of 3 μ_B, localized on the Cr atom. Comparison between the experimental and computed electronic structure for the ground and excited states shows that hybrid DFT is essential to correctly describe the electronic and optical properties of the doped system, with HSE predicting qualitatively similar features to SRSH but blue shifted in energy. The dopant leads to five in-gap states; within the majority spin manifold, three are singly occupied stemming from the hybridization between Cr-d states and host N-p and two unoccupied Cr-d states. The formation of these hybridized bands within the intrinsic gap of the host GaN results in the Cr: GaN band gap narrowing from 3.5 to 2.1 eV and multiple low-energy optical transitions: two weakly allowed transitions within the infrared region followed by a set of bright transitions in the visible window. The bright transitions from 1.78 to 2.17 eV are of mixed defect-

bulk character with the energy in excellent agreement with measurement. In addition, we investigated the electronic structure and optical properties of positively and negatively charged Cr dopants, and determined that the charge transition levels are in gap. Our results indicate the Cr-doped GaN has advantages for optoelectronic devices besides the well-known spintronic applications due to its visible light absorption.

[1] A. Y. Polyakov, N. B. Smirnov, A. V. Govorkov, N. V. Pashkova, A. A. Shlensky, S. J. Pearton, M. E. Overberg, C. R. Abernathy, J. M. Zavada, and R. G. Wilson, J. Appl. Phys. **93**, 5388 (2003).

[2] G. P. Das, B. K. Rao, and P. Jena, Phys. Rev. B **69**, 214422 (2004).

[3] Y. Li, W. Fan, H. Sun, X. Cheng, P. Li, X. Zhao, and M. Jiang, J. Solid State Chem. **183**, 2662 (2010).

[4] H. X. Liu, S. Y. Wu, R. K. Singh, L. Gu, D. J. Smith, N. Newman, N. R. Dilley, L. Montes, and M. B. Simmonds, Appl. Phys. Lett. **85**, 4076 (2004).

[5] J. Wang, P. Chen, X. Guo, Z. Li, and W. Lu, J. Cryst. Growth **275**, 393 (2005).

[6] N. Tandon, G. P. Das, and A. Kshirsagar, J. Phys.: Condens. Matter **18**, 9245 (2006).

[7] S. Sonoda, Appl. Phys. Lett. **100**, 202101 (2012).

[8] J. Baur, U. Kaufmann, M. Kunzer, J. Schneider, H. Amano, I. Akasaki, T. Detchprohm, and K. Hiramatsu, Appl. Phys. Lett. **67**, 1140 (1995).

[9] F. Zimmermann, G. Gärtner, H. Sträter, C. Röder, M. Barchuk, D. Bastin, P. Hofmann, M. Krupinski, T. Mikolajick, J. Heitmann, and F. Beyer, J. Lumin. **207**, 507 (2019).

[10] W. F. Koehl, B. Diler, S. J. Whiteley, A. Bourassa, N. T. Son, E. Janzén, and D. D. Awschalom, Phys. Rev. B **95**, 035207 (2017).

[11] M. van Schilfgaarde and O. N. Mryasov, Phys. Rev. B **63**, 233205 (2001).

[12] B. Xu and B. C. Pan, J. Appl. Phys. **105**, 103710 (2009).

[13] J. S. Lee, J. D. Lim, Z. G. Khim, Y. D. Park, S. J. Pearton, and S. N. G. Chu, J. Appl. Phys. **93**, 4512 (2003).

[14] N. Tandon, G. P. Das, and A. Kshirsagar, Phys. Rev. B **77**, 205206 (2008).

[15] B. J. Baliga, Semicond. Sci. Technol. **28**, 074011 (2013).

[16] J. Xu, A. Habib, S. Kumar, F. Wu, R. Sundararaman, and Y. Ping, Nat. Commun. **11**, 2780 (2020).

[17] R. Heitz, P. Thurian, I. Loa, L. Eckey, A. Hoffmann, I. Broser, K. Pressel, B. K. Meyer, and E. N. Mokhov, Phys. Rev. B **52**, 16508 (1995).

[18] T. Takeuchi, Y. Harada, T. Tokushima, M. Taguchi, Y. Takata, A. Chainani, J. J. Kim, H. Makino, T. Yao, T. Yamamoto, T. Tsukamoto, S. Shin, and K. Kobayashi, Phys. Rev. B **70**, 245323 (2004).

[19] X. Y. Cui, J. E. Medvedeva, B. Delley, A. J. Freeman, and C. Stampfl, Phys. Rev. B **75**, 155205 (2007).

[20] A. Ruzsinszky, J. P. Perdew, G. I. Csonka, O. A. Vydrov, and G. E. Scuseria, J. Chem. Phys. **126**, 104102 (2007).

[21] G. Onida, L. Reining, and A. Rubio, Rev. Mod. Phys. **74**, 601 (2002).

[22] A. Stroppa and G. Kresse, Phys. Rev. B **79**, 201201(R) (2009).

[23] D. K. Lewis, A. Ramasubramaniam, and S. Sharifzadeh, Phys. Rev. Mater. **4**, 063803 (2020).

[24] D. Wing, J. B. Haber, R. Noff, B. Barker, D. A. Egger, A. Ramasubramaniam, S. G. Louie, J. B. Neaton, and L. Kronik, Phys. Rev. Mater. **3**, 064603 (2019).

[25] A. Ramasubramaniam, D. Wing, and L. Kronik, Phys. Rev. Mater. **3**, 084007 (2019).

[26] M. S. Hybertsen and S. G. Louie, Phys. Rev. B **34**, 5390 (1986).

[27] G. Kresse and J. Furthmüller, Phys. Rev. B **54**, 11169 (1996).

[28] P. E. Blöchl, Phys. Rev. B **50**, 17953 (1994).

[29] J. Heyd, G. E. Scuseria, and M. Ernzerhof, J. Chem. Phys. **118**, 8207 (2003).

[30] D. K. Lewis, M. Matsubara, E. Bellotti, and S. Sharifzadeh, Phys. Rev. B **96**, 235203 (2017).

[31] B. Monemar, Phys. Rev. B **10**, 676 (1974).

[32] D. K. Lewis and S. Sharifzadeh, Phys. Rev. Mater. **3**, 114601 (2019).

[33] O. Lagerstedt and B. Monemar, Phys. Rev. B **19**, 3064 (1979).

[34] J. J. Kim, H. Makino, M. Sakurai, D. C. Oh, T. Hanada, M. W. Cho, T. Yao, S. Emura, and K. Kobayashi, J. Vacuum Sci. Technol. B **23**, 1308 (2005).

[35] Y. Hinuma, G. Pizzi, Y. Kumagai, F. Oba, and I. Tanaka, Comput. Mater. Sci. **128**, 140 (2017).

[36] G. Pizzi, V. Vitale, R. Arita, S. Blügel, F. Freimuth, G. Géranton, M. Gibertini, D. Gresch, C. Johnson, T. Koretsune, J. Ibañez-Azpiroz, H. Lee, J.-M. Lihm, D. Marchand, A. Marrazzo, Y. Mokrousov, J. I. Mustafa, Y. Nohara, Y. Nomura, L. Paulatto *et al.*, J. Phys.: Condens. Matter **32**, 165902 (2020).

[37] W. Tang, E. Sanville, and G. Henkelman, J. Phys.: Condens. Matter **21**, 084204 (2009).

[38] I. Choudhuri and D. G. Truhlar, J. Chem. Theory Comput. **16**, 5884 (2020).

[39] G. Henkelman, A. Arnaldsson, and H. Jónsson, Comput. Mater. Sci. **36**, 354 (2006).

[40] E. Sanville, S. D. Kenny, R. Smith, and G. Henkelman, J. Comput. Chem. **28**, 899 (2007).

[41] J. Wang and X.-Q. Gong, Appl. Surf. Sci. **428**, 377 (2018).

[42] P. Erhart, K. Albe, and A. Klein, Phys. Rev. B **73**, 205203 (2006).

[43] D. Koch and S. Manzhos, J. Phys. Chem. Lett. **8**, 1593 (2017).

[44] I. Tamblyn, S. Refaely-Abramson, J. B. Neaton, and L. Kronik, J. Phys. Chem. Lett. **5**, 2734 (2014).

[45] S. Refaely-Abramson, S. Sharifzadeh, M. Jain, R. Baer, J. B. Neaton, and L. Kronik, Phys. Rev. B **88**, 081204(R) (2013).

[46] S. Bhandari, M. S. Cheung, E. Geva, L. Kronik, and B. D. Dunietz, J. Chem. Theory Comput. **14**, 6287 (2018).

[47] L. Kronik and S. Kümmel, Adv. Mater. **30**, 1706560 (2018).

[48] Z.-F. Liu, D. A. Egger, S. Refaely-Abramson, L. Kronik, and J. B. Neaton, J. Chem. Phys. **146**, 092326 (2017).

[49] T. Maruyama, Y. Miyajima, S. Cho, K. Akimoto, and H. Kato, Phys. B: Condens. Matter **262**, 240 (1999).

[50] T. Maruyama, Y. Miyajima, K. Hata, S. H. Cho, K. Akimoto, H. Okumura, S. Yoshida, and H. Kato, J. Electron. Mater. **27**, 200 (1998).

[51] See Supplemental Material at http://link.aps.org/supplemental/10.1103/PhysRevB.107.184103 for more details about the structure of the doped GaN; the impact of the DFT functional on electronic structure; the nature of low-energy excitons in the presence of the defect; details regarding charged defect calculations; the accuracy of SRSH in capturing GaN d-band energetics; and details of thermodynamic transition level calculations.

[52] C. G. Van de Walle and J. Neugebauer, Nature (London) **423**, 626 (2003).

[53] S. V. Streltsov and D. I. Khomskii, Phys. Usp. **60**, 1121 (2017).

[54] M. J. I. Khan, J. Liu, Z. Kanwal, M. I. Khan, M. N. Usmani, and A. U. R. Khalid, Mater. Res. Expr. **7**, 055904 (2020).

[55] J. Heyd and G. E. Scuseria, J. Chem. Phys. **121**, 1187 (2004).

[56] A. V. Krukau, O. A. Vydrov, A. F. Izmaylov, and G. E. Scuseria, J. Chem. Phys. **125**, 224106 (2006).

[57] M. Mansouri, D. Casanova, P. Koval, and D. Sánchez-Portal, New J. Phys. **23**, 093027 (2021).

[58] G. Yu, G. Wang, H. Ishikawa, M. Umeno, T. Soga, T. Egawa, J. Watanabe, and T. Jimbo, Appl. Phys. Lett. **70**, 3209 (1997).

[59] Z.-h. Yang, F. Sottile, and C. A. Ullrich, Phys. Rev. B **92**, 035202 (2015).

[60] C. Freysoldt, J. Neugebauer, and C. G. Van de Walle, Phys. Rev. Lett. **102**, 016402 (2009).

[61] C. Freysoldt, J. Neugebauer, and C. G. Van de Walle, Phys. Stat. Solidi B **248**, 1067 (2011).

[62] J. Towns, T. Cockerill, M. Dahan, I. Foster, K. Gaither, A. Grimshaw, V. Hazlewood, S. Lathrop, D. Lifka, G. D. Peterson, R. Roskies, J. R. Scott, and N. Wilkins-Diehr, Comput. Sci. Eng. **16**, 62 (2014).